nature neuroscience

Imagined gait modulates neuronal network dynamics in the human pedunculopontine nucleus

Timothy L Tattersall[1], Peter G Stratton[1], Terry J Coyne[2], Raymond Cook[3], Paul Silberstein[3], Peter A Silburn[4], François Windels[1] & Pankaj Sah[1]

The pedunculopontine nucleus (PPN) is a part of the mesencephalic locomotor region and is thought to be important for the initiation and maintenance of gait. Lesions of the PPN induce gait deficits, and the PPN has therefore emerged as a target for deep brain stimulation for the control of gait and postural disability. However, the role of the PPN in gait control is not understood. Using extracellular single-unit recordings in awake patients, we found that neurons in the PPN discharged as synchronous functional networks whose activity was phase locked to alpha oscillations. Neurons in the PPN responded to limb movement and imagined gait by dynamically changing network activity and decreasing alpha phase locking. Our results indicate that different synchronous networks are activated during initial motor planning and actual motion, and suggest that changes in gait initiation in Parkinson's disease may result from disrupted network activity in the PPN.

Parkinson's disease is a progressive neurodegenerative disorder characterized by bradykinesia, rigidity and tremor, and is thought to result from a loss of dopaminergic neurons[1]. Treatment of Parkinson's disease is symptomatic, with dopamine replacement with levodopa being the mainstay of treatment[2]. However, after an initial period of improvement, the beneficial effects of levodopa are overshadowed by side effects such as dyskinesia and neuropsychiatric complications[3]. Moreover, in advanced Parkinson's disease, axial symptoms such as freezing of gait and postural difficulties become increasingly prevalent. Although the motor symptoms of Parkinson's disease are responsive to dopamine replacement, gait freezing and postural instability respond poorly. The pathophysiology of these gait disturbances is poorly understood, but their late onset and resistance to levodopa has led to the suggestion that they may result from pathology in non-dopaminergic structures involved in locomotion[4,5].

Gait is controlled by genetically defined neuronal networks, the central pattern generators (CPGs), in the spinal cord[6,7], which are in turn activated by supraspinal centers that initiate and control movement[6–8]. Among these, the mesencepalic locomotor region (MLR) in the brainstem is important for the control of gait[9,10]. In the MLR, the PPN, which is extensively connected with the basal ganglia[11], has a central role in the initiation and maintenance of gait[12–14] and lesions of the PPN induce gait deficits[14]. Gait and postural disturbances in Parkinson's disease are accompanied by cell loss in the PPN[14–16], but are partially relieved by deep brain stimulation (DBS) in the PPN[17–19], supporting the central role of the PPN in locomotion.

Much is understood about the development and function of spinal cord CPGs[20]. However, although CPG function is controlled by afferent projections from the MLR[9,10], little is understood about activity in the MLR and its response to movement. Using single-unit recordings in awake patients, we examined the properties of neurons in the human PPN and their response to limb movement and imagined gait. We found that neurons in the PPN formed networks of neurons that discharged synchronously, and different networks were engaged during limb movement and imagined gait. It is generally believed that motor planning is initiated in parietal, premotor and supplementary motor areas, and this activity is fed to brainstem centers for control of movement[21,22]. Our results indicate that networks of neurons in the PPN are also engaged during motor planning, and these networks are modulated by proprioceptive feedback, suggesting that the PPN is involved in both the initiation and control of movement.

RESULTS

Recordings were obtained from the PPN in 11 adults (mean age = 74 years; 8 males, 3 females), ten of whom were diagnosed with Parkinson's disease and one with progressive supranuclear palsy. The PPN is defined as a collection of neurons in the caudal mesencephalic tegmentum[12,13,23] extending caudally from the substantia nigra to the locus coeruleus[12,23]. On the basis of cell density and neurochemical markers, the PPN is divided into the pars compacta (PPNc), which is located more caudally and contains a high density of cholinergic neurons, and pars dissipata (PPNd), which extends throughout the rostro-caudal axis of the nucleus[23,24]. As the PPN boundaries are not clearly identified in standard magnetic resonance images[25], we defined it as the region extending 12 mm caudally from the mid-inferior collicular plane (mid-IC) along the floor of the fourth ventricle[23,26,27] (**Fig. 1a–d**), and divided it into three regions (rostral, mid and caudal-PPN), each extending 4 mm caudally from the mid-IC plane (**Fig. 1d**).

A total of 676 units were isolated (**Fig. 1e** and Online Methods), with 120 in the rostral-PPN, 265 in the mid-PPN and 291 in the

[1]Queensland Brain Institute, The University of Queensland, Brisbane, Queensland, Australia. [2]St. Andrews Hospital and University of Queensland, Brisbane, Queensland, Australia. [3]Royal North Shore and North Shore Private Hospitals, Sydney, New South Wales, Australia. [4]Centre for Clinical Research, Royal Brisbane and Women's Hospital, University of Queensland, Herston, Queensland, Australia. Correspondence should be addressed to P. Sah (pankaj.sah@uq.edu.au).

Received 22 August 2013; accepted 2 January 2014; published online 2 February 2014; doi:10.1038/nn.3642

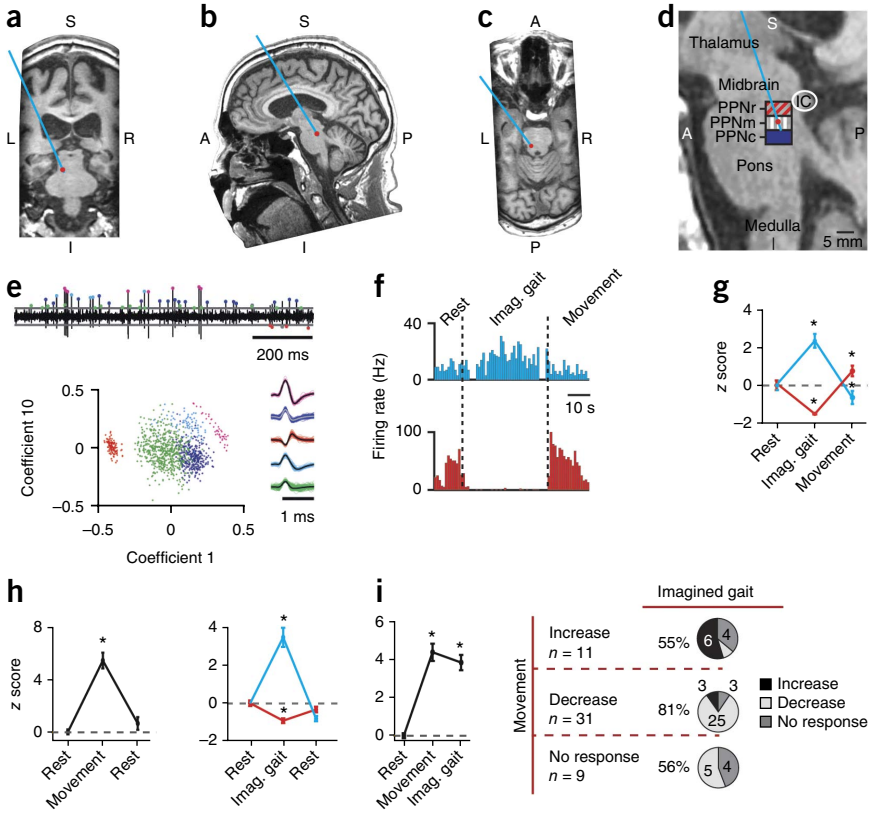

Figure 1 Single units in the human PPN respond to both passive movement and imagined gait. (**a**–**c**) Targeting of electrodes in the human PPN. T1-weighted magnetic resonance images, oriented to the anterior commissure–posterior commissure line, from one patient are shown in coronal (**a**), sagittal (**b**) and axial (**c**) slices. A, anterior; P, posterior; L, left; R, right; I, inferior; S, superior. (**d**) Sagittal T1-weighted magnetic resonance image showing the location of the PPN, which extends 12 mm below the center of the inferior colliculus (IC). The rostral-PPN (PPNr, red diagonal lines), mid-PPN (PPNm, white vertical lines) and caudal PPN (PPNc, dark blue) regions are shown. Image is oriented to the floor of the fourth ventricle. The microelectrode trajectory is indicated by the blue line and a recording site in the mid-PPN is marked by the red dot. (**e**) Extracellular unit activity recorded from the mid-PPN. Five distinct units, marked by different colors, could be isolated, as shown in the lower panel. Units are plotted against the indicated wavelet coefficients and each cluster is marked by a different color. The mean shape of each unit is shown in the inset. (**f**) Recording in the caudal-PPN with two identified neurons (red and blue). The instantaneous firing rate of each neuron is shown at rest, during imagined gait and during passive movement of the contralateral leg. One neuron (blue) responded with an increase in discharge during imagined gait, which then returned to near baseline levels during passive movement. The other neuron (red unit) was inhibited during imagined gait, but then recovered its activity during passive movement. (**g**) Mean *z* scores, normalized to the resting state, are shown for each of the three conditions for both units. (**h**) Neuronal discharge was modulated by behavioral state, but then returned to baseline. Left, the response of a single unit to passive movement; this unit increased its firing in response to movement. Right, two isolated units (red, blue). The red unit was inhibited during imagined gait, but the blue unit was excited. (**i**) Left, normalized *z* score of discharge rate for a neuron that was activated during both passive movement and imagined gait. Right, summary of response of narrow units to both passive movement and imagined gait. Pie charts show the responses to imagined gait for units that had increased firing during passive movement (top), for units that had decreased firing during passive movement (middle), and for units that did not respond to passive movement (bottom). $^*P < 0.05$. All error bars represent ±s.e.m.

caudal-PPN. Single units were accepted for analysis if they had a signal-to-noise ratio greater than 4 and autocorrelograms showed a clear refractory period of >1 ms (**Supplementary Fig. 1a**). Neurons were divided into two populations (**Supplementary Fig. 1b**): narrow-spike units (87%, 588 of 676) having a spike width of 176 ± 0.9 μs and wide-spike units (13%, 88 of 676) with a spike width of 254 ± 3.1 μs. Narrow and wide units did not differ significantly ($P = 0.46$, rank sum test) in mean firing rate (12.2 ± 0.7 Hz versus 13.1 ± 3.8 Hz; **Supplementary Fig. 1c**), but narrow-spike units had low levels of burst activity, with only 16 ± 2% of spikes occurring in bursts. In comparison, wide-spike units had a significantly greater burst activity (**Supplementary Fig. 1c**) on all four measures of bursting (Online Methods), with 46 ± 7% of spikes occurring in bursts ($P < 0.001$, medians: 1% versus 48%, rank sum test). Wide-spike units comprised 18% of units in the caudal-PPN, but comprised significantly lower proportions in the mid (10%) and rostral-PPN (9%) ($P = 0.005$, Fisher's exact test; **Supplementary Fig. 1d**). The PPN contains cholinergic, GABAergic and glutamatergic neurons[28–31], and, given that cholinergic cells have wider action potentials[23] and are more prevalent in the caudal PPN[30,31], it is likely that wide-spike neurons are cholinergic.

PPN neurons respond to limb movement and imagined gait

The PPN is extensively connected with the basal ganglia and cerebellum and is thought to be important for the initiation and control of locomotion[12,13,32]. We first tested units for their response to passive movement of the lower limbs, involving flexion and extension of the ankle, knee and hip, as occurs during locomotion[30,33]. In total, 76 narrow-spike and 10 wide-spike neurons were tested. For narrow-spike units, 13 responded with an increase in discharge, whereas 36 were inhibited. For wide-spike units, only one responded with an increase in discharge, whereas four showed a decrease in discharge (**Supplementary Fig. 2**). Thus, the activity of neurons in the PPN, a region involved in gait control, is modulated during limb movement, a manipulation that provides proprioceptive inputs to the PPN[33].

To determine whether the PPN is involved in the initiation and planning of gait, we asked patients to close their eyes and imagine walking along a road. This is imagined gait[34], where patients simply prepare to move, and a lack of movement during imagined gait was confirmed by the absence of electromyograph activity (**Supplementary Fig. 3**). Imagined gait had very similar effects as actual movement, with some neurons increasing their discharge and others being inhibited (**Fig. 1f**,**g**). Both narrow-spike (58 of 80) and wide-spike (9 of 14) units responded to imagined gait. For narrow-spike units, 14 responded with an increase in firing rate, whereas 44 had a reduction in firing during imagined gait. For wide-spike neurons, 2 of 14 increased their discharge during imagined gait and 7 of 14 were inhibited (**Supplementary Fig. 2**). Responses were limited to each manipulation, returning to resting levels following movement or imagined gait (**Fig. 1h**).

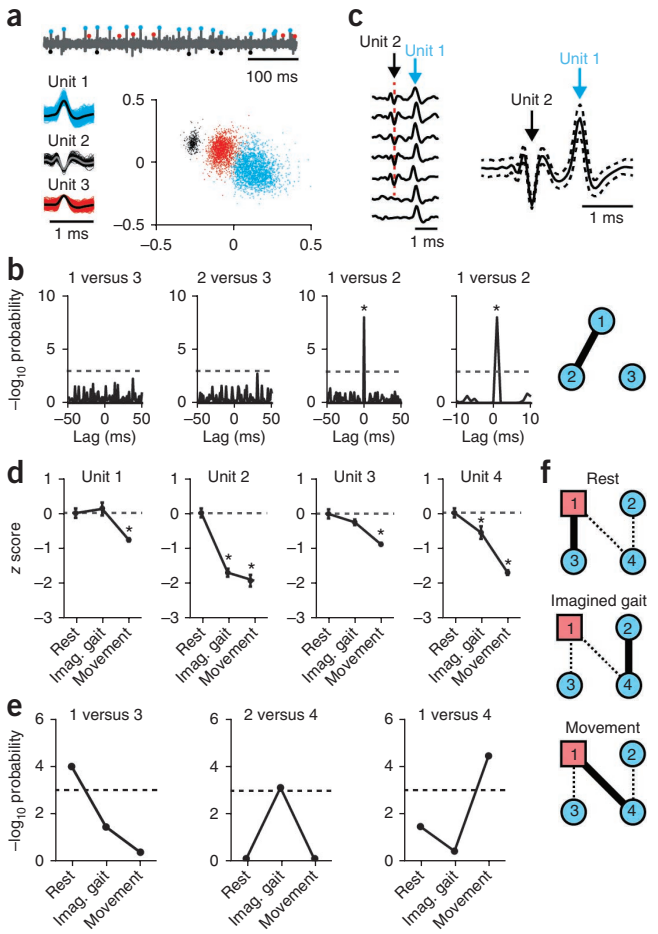

Figure 2 Distinct networks of neurons in the PPN are engaged during movement and imagined gait. (**a**) Recording in the mid-PPN in which three units can be isolated. Spike times for the three units (blue, black and red circles) are superimposed on the microelectrode recording trace. (**b**) Cross-correlograms indicate that units 1 and 2 showed significant correlated activity (*$P < 0.01$), but discharge of units 1 and 3, and units 2 and 3 were not correlated. It can be seen in the expanded cross-correlogram (rightmost panel) that the lag time for the cross-correlation was very brief. The network diagram for the three units is also shown. (**c**) Discharge of unit 1 almost always followed unit 2, with some failures, but the two units fired together on average, as shown on the right panel. The dashed line shows 1 s.d. beyond the mean. (**d**) Different recording (caudal-PPN) in which four units were isolated and tested for their responses to imagined gait and passive movement. With imagined gait, units 1 and 3 did not change their activity, but units 2 and 4 responded with a decrease in firing rate. During passive movement, all four units responded with a reduction in firing rate (*$P < 0.05$ rank sum test). (**e**) Network activity changed with passive movement and discharge rate. At rest, only units 1 and 3 showed correlated activity. During imagined gait, the activity of units 2 and 4 became correlated, but correlated activity between unit 1 and unit 3 was lost. During passive movement, only units 1 and 4 showed correlated activity. (**f**) Network diagrams showing correlated unit activity during rest, imagined gait and movement. Wide-spiking units are indicated by the red squares, and narrow-spiking neurons by blue circles. Thick lines joining represented units indicate significant correlations, and dotted lines indicate pairs of units that were not correlated when the network was in the current state, but were correlated when the network was in a different state. All error bars represent ±s.e.m.

These results indicate that neurons in the PPN not only respond to limb movement, when there is clear proprioceptive feedback, but also to imagined gait, when movement is planned, but not executed. We next asked whether motor planning might activate the same neurons as those engaged during limb movement. Indeed, some neurons responded to both real and imagined limb movement (**Fig. 1i**). For narrow-spike neurons, of 11 units that responded with an increase in activity during passive movement, six also increased their activity during imagined gait, one showed a decrease in activity and four did not respond during imagined gait. For units that were inhibited during limb movement ($n = 31$), 25 also decreased their activity during imagined gait, three had an increase in activity and three did not change. Thus, the PPN contains some neurons that respond similarly to both conditions, but they are few in number and the physiological importance of these neurons, if any, remains unclear.

State-dependent networks of neurons in the PPN

Cross-correlation analysis revealed substantial correlated activity in many neuron pairs (**Fig. 2**). Correlated discharge was prevalent in the caudal-PPN and mid-PPN, with significant correlated activity ($P < 0.01$) in 48 of 453 pairs and 29 of 246 pairs, respectively. In the rostral-PPN, 2 of 47 pairs of neurons had correlated activity. In most correlated pairs, the lag time between units was short (1–2 ms; **Fig. 2b**,**c**), indicating that neurons in the PPN can discharge with millisecond precision. Correlated activity was seen between all three combinations of narrow and wide-spike units, but more commonly involved wide-spike units. Of the 523 narrow-narrow pairs tested, 49 showed significant correlated firing, whereas 22 of 193 wide-narrow pairs tested and 8 of 30 wide-wide pairs tested showed correlated activity. Moreover, in 28 recordings in which more than two units were detected at a single site, correlated activity was seen between several pairs of neurons, indicating that neurons in the PPN discharge as networks (**Supplementary Fig. 4**).

Active networks in the PPN changed with movement and imagined gait. In one example (**Fig. 2d–f**), four units were isolated, and at rest units 1 and 3 fired in synchrony. During imagined gait, the activity of two neurons (units 1 and 3) did not change, but activity was inhibited in units 2 and 4 (**Fig. 2d**). In parallel, units 1 and 3, which discharged synchronously at rest, lost their correlated activity, whereas units 2 and 4, whose activity levels did not change, fired in synchrony (**Fig. 2e**,**f**). During passive movement, the response of this network was entirely different, with all four neurons showing a decrease in activity. Moreover, despite the reduced activity, two of the neurons (units 1 and 4) now fired synchronously, whereas activity in the other neurons was uncorrelated. Thus, imagined gait and passive movement change the patterns of network activity establishing distinct network states. For neurons tested during imagined gait, 23 pairs had significant correlated firing during baseline. Of these, 20 pairs showed a decrease in correlated firing during imagined gait, but a small proportion (3 of 23 pairs) had an increase in correlated firing. Similarly, for passive movement, 32 pairs of neurons showed correlated firing during baseline, of which 20 pairs had decreased correlated firing during movement, eight had increased correlated firing and four pairs remained unchanged.

There was no correlation between changes in network connectivity and changes in firing rate. For the 20 pairs of neurons showing a decrease in correlation strength during imagined gait, both neurons did not change their firing rate in four pairs, both neurons decreased their activity in 12 pairs, one neuron increased and one decreased activity in one pair, one neuron decreased activity and one neuron was unchanged in one pair, and, in two pairs, one neuron increased activity while the other was unchanged. During movement, for the 20 pairs of neurons showing a decrease in correlation strength, three pairs did not change their firing rate, three pairs had an increase in

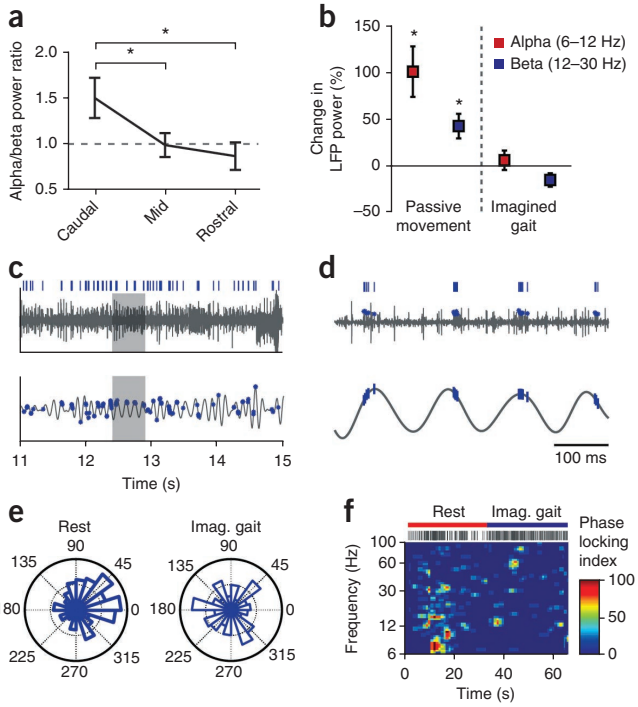

Figure 3 LFP oscillation is more prevalent in caudal PPN and phase locks neural activity. (**a**) Ratio of alpha (6–12 Hz) to beta (12–30 Hz) LFP power in each PPN region. Data are presented as mean ± s.e.m. There was significantly greater alpha power relative to beta in the caudal-PPN compared with the mid and rostral-PPN (*$P = 0.001$). (**b**) Changes in LFP power in the caudal PPN during passive movement and imagined gait. Passive movement induced significant increases in alpha (*$P = 0.001$) and beta (*$P = 0.004$) power, whereas imagined gait was not associated with a significant change in alpha or beta power. Data are presented as mean ± s.e.m. ($n = 19$ recordings for passive movement, $n = 22$ recordings for imagined gait). (**c**) Raw unfiltered recording is shown (top) and the same recording band-pass filtered to the alpha band (bottom). The shaded region shows one instance of increased alpha band oscillations. Spike times of one of the six identified neurons (wide-spike neuron) in the recording are shown as rasters (top) and dots (bottom). (**d**) Enlarged view of 0.5 s of activity (shaded region in **c**) showing strong phase locking of the spike times to the peaks of the alpha oscillations. (**e**) Polar plot of the LFP phases at the times of neuronal discharge for the rest period shown in **c**, indicating significant phase locking ($P < 0.001$ Rayleigh test) near the peak (0°) (left). During imagined gait (right), there was no significant phase locking ($P = 0.064$). (**f**) Testing all combinations of time and frequency windows across the recording (Online Methods) revealed periods of strong phase locking for this unit during rest and much reduced locking during imagined gait.

firing rate of both neurons, nine pairs had a decrease in firing rate of both neurons, four pairs had one neuron that decreased activity and one that did not change, and one pair had one neuron that increased activity and one neuron that did not change.

Together, these results show that neurons in the PPN discharge in networks that change during passive movement and imagined gait. Moreover, although there are some shared neurons between networks engaged in the two conditions, the activity of these neurons can be differentially modulated in the two states, indicating that the networks recruited during movement and imagined gait are different.

Phase locking in the PPN is state dependent

Local field potential (LFP) recordings from the PPN have reported oscillations in both the alpha (6–12 Hz) and beta (12–30 Hz) frequency bands[33,35–37], with relatively higher alpha power in caudal-PPN and higher beta power in the rostral-PPN[35]. Active gait is accompanied by increased LFP alpha power in the caudal PPN[35]. Consistent with this, we also found that alpha power was significantly higher relative to beta power in caudal PPN (**Fig. 3a**), with a mean alpha/beta power ratio of 0.86 ± 0.15 in rostral-PPN, 0.99 ± 0.13 in mid-PPN and 1.50 ± 0.22 in the caudal-PPN ($P < 0.001$, Kruskal-Wallis test). During limb movement, there was an increase in both alpha and beta power (**Fig. 3b**), with an overall increase the in alpha/beta power ratio in the caudal PPN from 1.98 ± 0.47 to 2.79 ± 0.73 ($n = 19$). During imagined gait, the effects on alpha and beta LFP power were smaller (**Fig. 3b**), but the overall change in the alpha/beta power ratio was similar to that seen during passive movement, with an increase from 1.99 ± 0.40 to 2.58 ± 0.53 ($n = 22$). The LFP results in part from local neuronal activity[35], and we next tested the relationship between unit activity and LFP oscillations. At rest, 75 of 695 neurons tested were significantly phase locked in the alpha (6–12 Hz) frequency band (Rayleigh test, $P < 0.01$; **Fig. 3c–f**). Phase locking was evident in all three regions: caudal-PPN (23 of 301), mid-PPN (39 of 271) and rostral-PPN (13 of 123). During both limb movement and imagined gait, phase locking in the caudal PPN was significantly reduced (**Fig. 3e,f**), with a decrease in the median phase locking index by 19% for movement ($P < 0.05$) and 29% ($P < 0.001$) for imagined gait.

DISCUSSION

The PPN, which is located in the ponto-mesencephalic tegmentum, is part of the mesencephalic locomotor region and is involved in the initiation and control of gait[12,13]. Stimulation of the PPN induces spontaneous locomotion, and lesions of the PPN result in gait deficits[14]. Thus, the PPN has emerged as a target for DBS to control freezing of gait and postural instability that appear in advanced Parkinson's disease[38].

The PPN contains a mixed population of cholinergic, glutamatergic and GABAergic neurons[11,13,23,29]. Electrophysiologically, at least three types of neuron have been identified[31,33,39], but there is little correlation between cells' electrophysiological properties and their neurochemical identity. Cholinergic neurons are more prevalent in the caudal PPN, and the presence of gait disorders has been correlated with the loss of these cells[14–16]. Given that wide-spike neurons had a substantially lower density than narrow-spike neurons, and were more common in the caudal PPN, these cells are likely to be cholinergic neurons[40].

Limb movement and imagined gait had diverse effects on neural activity in the PPN[33], but resulted in an overall reduction in activity. The PPN has extensive connections with the basal ganglia[5,11], receiving strong inhibitory inputs from both the globus pallidus internus and substantia nigra[41]. Thus, the reduction in PPN activity may be mediated by inhibitory input from the basal ganglia[41]. Responses to limb movement have also been reported in the STN[42]; given that the PPN is thought to be involved in gait, it would be interesting to compare the responses of these two nuclei to distinct movements of the upper and lower limbs. Many neurons in the PPN showed highly correlated activity, resulting in networks of neurons that discharged synchronously. Limb movement and imagined gait changed the patterns of correlated activity, establishing distinct network states during limb movement and imagined gait. These results suggest that the PPN is not simply a relay station between the basal ganglia and spinal cord CPGs, but is also involved in gait initiation.

Alpha band LFP activity in the PPN[33,35] increases during locomotion[35]. Consistent with this, LFP alpha power in the caudal PPN increased during limb movement. Although imagined gait had little effect on alpha power, both manipulations resulted in decreased alpha phase locking. Thus, movement and imagined gait both modulate PPN activity with an overall uncoupling of neuronal discharge from alpha oscillations. The fact that passive movement and imagined gait have distinct effects on LFP power and activate distinct networks of neurons indicates that these two states activate the PPN via different circuits. Passive movement activates sensory and proprioceptive afferent feedback that is essential for accurate locomotion[8]. In contrast, imagined gait involves preparation for movement[43] and, as it is not accompanied by limb movement or muscle activity, does not involve any sensory feedback. In the monkey PPN, neurons also respond to saccadic eye movement[44]. Although patients had their eyes closed during imagined gait, we cannot exclude some eye movement that may have contributed to the response during imagined gait. Motor planning is thought to arise in higher cortical areas such as parietal, premotor and supplementary motor areas[45], and movement is initiated and controlled by projections from these regions to brainstem and spinal cord central pattern generators[21,22], in concert with sensory feedback from the periphery. Our results suggest that the PPN, a component of the brainstem MLR, is not only involved in the control of movement, but has a role in motor planning. The similar response of some neurons to limb movement and imagined gait suggests repetition of activity during motor planning and movement, but the physiological role, if any, of such activity is not known.

Cholinergic neurons in the PPN make extensive local connections[46] and are preferentially coupled in correlated networks of activity. Parkinson's disease is accompanied by increased inhibitory drive from the basal ganglia, which would in turn reduce the activity of non-cholinergic neurons in the PPN. In combination with the reduced numbers of cholinergic neurons in the PPN[14–16], the disrupted recruitment of appropriate networks in the PPN may contribute to the gait disturbance seen in Parkinson's disease. It is therefore possible that DBS in the PPN, and the resultant changes in local synaptic transmission, may lead to changes in the networks that are active in planning and initiation of gait.

METHODS

Methods and any associated references are available in the online version of the paper.

Note: Any Supplementary Information and Source Data files are available in the online version of the paper.

ACKNOWLEDGMENTS

We are grateful to all of the patients for agreeing to participate in this study. We thank R. Tweedale and P. Martin for comments on the manuscript. This work was supported by grants from the Australian National Health and Medical Research Council and Australian Research Council.

AUTHOR CONTRIBUTIONS

T.J.C. and R.C. performed all of the surgical procedures. P.A.S. and P. Silberstein recruited patients and chose targets for recording, and performed all of the intraoperative clinical assessment. T.L.T. collected and analyzed data and wrote the manuscript. F.W. collected and analyzed data. P.G.S. helped to analyze the data. P. Sah analyzed the data and wrote the manuscript.

COMPETING FINANCIAL INTERESTS

The authors declare no competing financial interests.

1. Willis, G.L., Moore, C. & Armstrong, S.M. Breaking away from dopamine deficiency: an essential new direction for Parkinson's disease. *Rev. Neurosci.* **23**, 403–428 (2012).
2. Fernandez, H.H. Updates in the medical management of Parkinson disease. *Cleve. Clin. J. Med.* **79**, 28–35 (2012).
3. Weintraub, D. Dopamine and impulse control disorders in Parkinson's disease. *Ann. Neurol.* **64** (suppl. 2): S93–S100 (2008).
4. Bonnet, A.M., Loria, Y., Saint-Hilaire, M.H., Lhermitte, F. & Agid, Y. Does long-term aggravation of Parkinson's disease result from nondopaminergic lesions? *Neurology* **37**, 1539–1542 (1987).
5. Pahapill, P.A. & Lozano, A.M. The pedunculopontine nucleus and Parkinson's disease. *Brain* **123**, 1767–1783 (2000).
6. Grillner, S. Biological pattern generation: the cellular and computational logic of networks in motion. *Neuron* **52**, 751–766 (2006).
7. Armstrong, D.M. The supraspinal control of mammalian locomotion. *J. Physiol. (Lond.)* **405**, 1–37 (1988).
8. Rossignol, S., Dubuc, R. & Gossard, J.P. Dynamic sensorimotor interactions in locomotion. *Physiol. Rev.* **86**, 89–154 (2006).
9. Garcia-Rill, E., Skinner, R.D. & Fitzgerald, J.A. Activity in the mesencephalic locomotor region during locomotion. *Exp. Neurol.* **82**, 609–622 (1983).
10. Jahn, K. *et al.* Supraspinal locomotor control in quadrupeds and humans. *Prog. Brain Res.* **171**, 353–362 (2008).
11. Martinez-Gonzalez, C., Bolam, J.P. & Mena-Segovia, J. Topographical organization of the pedunculopontine nucleus. *Front. Neuroanat.* **5**, 22 (2011).
12. Garcia-Rill, E. The pedunculopontine nucleus. *Prog. Neurobiol.* **36**, 363–389 (1991).
13. Winn, P.J. How best to consider the structure and function of the pedunculopontine tegmental nucleus: evidence from animal studies. *Neurol. Sci.* **248**, 234–250 (2006).
14. Karachi, C. *et al.* Cholinergic mesencephalic neurons are involved in gait and postural disorders in Parkinson disease. *J. Clin. Invest.* **120**, 2745–2754 (2010).
15. Zweig, R.M., Jankel, W.R., Hedreen, J.C., Mayeux, R. & Price, D.L. The pedunculopontine nucleus in Parkinson's disease. *Ann. Neurol.* **26**, 41–46 (1989).
16. Hirsch, E.C., Graybiel, A.M., Duyckaerts, C. & Javoy-Agid, F. Neuronal loss in the pedunculopontine tegmental nucleus in Parkinson disease and in progressive supranuclear palsy. *Proc. Natl. Acad. Sci. USA* **84**, 5976–5980 (1987).
17. Jenkinson, N. *et al.* Anatomy, physiology, and pathophysiology of the pedunculopontine nucleus. *Mov. Disord.* **24**, 319–328 (2009).
18. Thevathasan, W. *et al.* A spatiotemporal analysis of gait freezing and the impact of pedunculopontine nucleus stimulation. *Brain* **135**, 1446–1454 (2012).
19. Mazzone, P. *et al.* Implantation of human pedunculopontine nucleus: a safe and clinically relevant target in Parkinson's disease. *Neuroreport* **16**, 1877–1881 (2005).
20. Goulding, M. Circuits controlling vertebrate locomotion: moving in a new direction. *Nat. Rev. Neurosci.* **10**, 507–518 (2009).
21. Iseki, K., Hanakawa, T., Shinozaki, J., Nankaku, M. & Fukuyama, H. Neural mechanisms involved in mental imagery and observation of gait. *Neuroimage* **41**, 1021–1031 (2008).
22. Andersen, R.A. & Cui, H. Intention, action planning, and decision making in parietal-frontal circuits. *Neuron* **63**, 568–583 (2009).
23. Mesulam, M.M., Geula, C., Bothwell, M.A. & Hersh, L.B. Human reticular formation: cholinergic neurons of the pedunculopontine and laterodorsal tegmental nuclei and some cytochemical comparisons to forebrain cholinergic neurons. *J. Comp. Neurol.* **283**, 611–633 (1989).
24. Olszewski, J. & Baxter, D. *Cytoarchitecture of the Human Brainstem* (Lippencott, Philadelphia, 1954).
25. Mazzone, P., Sposato, S., Insola, A., Dilazzaro, V. & Scarnati, E. Stereotactic surgery of nucleus tegmenti pedunculopontine. *Br. J. Neurosurg.* **22** (suppl. 1): S33–S40 (2008).
26. Manaye, K.F. *et al.* Quantification of cholinergic and select non-cholinergic mesopontine neuronal populations in the human brain. *Neuroscience* **89**, 759–770 (1999).
27. Paxinos, G. & Huang, X.F. *Atlas of the Human Brainstem* (Academic Press, London, 1995).
28. Kang, Y. & Kitai, S.T. Electrophysiological properties of pedunculopontine neurons and their postsynaptic responses following stimulation of substantia nigra reticulata. *Brain Res.* **535**, 79–95 (1990).
29. Koyama, Y., Honda, T., Kusakabe, M., Kayama, Y. & Sugiura, Y. *In vivo* electrophysiological distinction of histochemically identified cholinergic neurons using extracellular recording and labelling in rat laterodorsal tegmental nucleus. *Neuroscience* **83**, 1105–1112 (1998).
30. Matsumura, M., Watanabe, K. & Ohye, C. Single-unit activity in the primate nucleus tegmenti pedunculopontinus related to voluntary arm movement. *Neurosci. Res.* **28**, 155–165 (1997).
31. Takakusaki, K., Shiroyama, T. & Kitai, S.T. Two types of cholinergic neurons in the rat tegmental pedunculopontine nucleus: electrophysiological and morphological characterization. *Neuroscience* **79**, 1089–1109 (1997).

32. Garcia-Rill, E., Simon, C., Smith, K., Kezunovic, N. & Hyde, J. The pedunculopontine tegmental nucleus: from basic neuroscience to neurosurgical applications: arousal from slices to humans: implications for DBS. *J. Neural Transm.* **118**, 1397–1407 (2011).
33. Weinberger, M. *et al.* Pedunculopontine nucleus microelectrode recordings in movement disorder patients. *Exp. Brain Res.* **188**, 165–174 (2008).
34. Crémers, J., D'Ostilio, K., Stamatakis, J., Delvaux, V. & Garraux, G. Brain activation pattern related to gait disturbances in Parkinson's disease. *Mov. Disord.* **27**, 1498–1505 (2012).
35. Thevathasan, W. *et al.* Alpha oscillations in the pedunculopontine nucleus correlate with gait performance in parkinsonism. *Brain* **135**, 148–160 (2012).
36. Tsang, E.W. *et al.* Involvement of the human pedunculopontine nucleus region in voluntary movements. *Neurology* **75**, 950–959 (2010).
37. Shimamoto, S.A. *et al.* Physiological identification of the human pedunculopontine nucleus. *J. Neurol. Neurosurg. Psychiatry* **81**, 80–86 (2010).
38. Lozano, A.M. & Lipsman, N. Probing and regulating dysfunctional circuits using deep brain stimulation. *Neuron* **77**, 406–424 (2013).
39. Kamondi, A., Williams, J.A., Hutcheon, B. & Reiner, P.B. Membrane properties of mesopontine cholinergic neurons studied with the whole-cell patch-clamp technique: implications for behavioral state control. *J. Neurophysiol.* **68**, 1359–1372 (1992).
40. Dormont, J.F., Conde, H. & Farin, D. The role of the pedunculopontine tegmental nucleus in relation to conditioned motor performance in the cat. I. Context-dependent and reinforcement-related single unit activity. *Exp. Brain Res.* **121**, 401–410 (1998).
41. Takakusaki, K., Habaguchi, T., Ohtinata-Sugimoto, J., Saitoh, K. & Sakamoto, T. Basal ganglia efferents to the brainstem centers controlling postural muscle tone and locomotion: a new concept for understanding motor disorders in basal ganglia dysfunction. *Neuroscience* **119**, 293–308 (2003).
42. Hutchison, W.D. *et al.* Neurophysiological identification of the subthalamic nucleus in surgery for Parkinson's disease. *Ann. Neurol.* **44**, 622–628 (1998).
43. Jeannerod, M. & Decety, J. Mental motor imagery: a window into the representational stages of action. *Curr. Opin. Neurobiol.* **5**, 727–732 (1995).
44. Kobayashi, Y., Inoue, Y., Yamamoto, M., Isa, T. & Aizawa, H. Contribution of pedunculopontine tegmental nucleus neurons to performance of visually guided saccade tasks in monkeys. *J. Neurophysiol.* **88**, 715–731 (2002).
45. Jahn, K. *et al.* Imaging human supraspinal locomotor centers in brainstem and cerebellum. *Neuroimage* **39**, 786–792 (2008).
46. Mena-Segovia, J., Sims, H.M., Magill, P.J. & Bolam, J.P. Cholinergic brainstem neurons modulate cortical gamma activity during slow oscillations. *J. Physiol. (Lond.)* **586**, 2947–2960 (2008).

ONLINE METHODS

Subjects. This report is based on 11 patients, ten with Parkinson's disease and one with progressive supranuclear palsy, who were implanted with bilateral DBS electrodes in the PPN region. The indications for PPN stimulation consisted of severe gait freezing and postural instability, persisting 'ON medication', and either causing frequent falls or precluding walking. Patients were recruited from a movement disorders clinic in Brisbane, Australia. Ethics committee approval was obtained from the University of Queensland Human Ethics Committee and all patients gave written informed consent. None of the patients had previously received ablative or DBS surgery.

Extracellular recordings were made from neurons in the PPN using microelectrodes (0.5–1 MΩ, 50-μm tip, FHC) along a trajectory starting at least 5 mm above the target and extending 5 mm below the target (in 1-mm increments). Patients were awake during recording. Signals were amplified, band-pass filtered (0.5–5 kHz, Butterworth filter) and digitally recorded (22 kHz) using a Leadpoint recording system (Medtronic). Recordings of at least 30-s duration were obtained at each site for offline analysis. In all patients, neural activity was recorded in the resting state, and in six patients, recordings were also made during imagined gait and passive movement. In imagined gait, patients lay supine on the surgical table and were asked to close their eyes and imagine walking along a road. All patients were questioned on their ability to imagine walking along the road the day before surgery and also in theatre following the recording, and responded positively. During passive movement, flexion and extension of the contralateral hip, knee and ankle were performed by a neurologist (P.A.S.).

Surgical procedure and targeting. Magnetic resonance brain images of each patient were obtained the day before surgery using a 3-T scanner (General Electric Signa HDxt). We obtained T1-weighted (1-mm isotropic voxels) and T2-weighted fluid-attenuated inversion-recovery (FLAIR, 1 × 1 × 2 mm voxels) images. On the morning of the surgery, patients were sedated with a continuous infusion of propofol for light sedation, and received local anesthetic to the scalp. A Cosman-Roberts-Wells head frame was fixed to the skull with pins. Stereotactic computed tomography images were obtained (1.25-mm slices, 0.625 × 0.625 mm in-slice resolution). T1-weighted and FLAIR magnetic resonance images were registered with computed tomography images using a mutual information technique (StealthStation Treon Plus, Medtronic). The anterior commissure, posterior commissure, and mid-sagittal landmarks were identified on FLAIR magnetic resonance images. Magnetic resonance and computed tomography images were aligned to the anterior commissure–posterior commissure line. The target was chosen 6 mm lateral to the mid-sagittal plane and 5–8 mm anterior to the floor of the fourth ventricle. The rostrocaudal position of the target was 8–12 mm caudal to the mid-point of the inferior colliculus, measured along the floor of the fourth ventricle. The frontal scalp was prepared and draped. A small bilateral scalp flap was raised, and bilateral burr holes were made at a location that avoided ventricular violation by the microelectrode or lead[47]. Microstimulation (30 Hz, 0.1-ms pulse width, 1.5 mA) was used to assess electrode location. Infusion of propofol was stopped at least 30 min before recordings and all patients were fully awake during the recording.

Localization of recording and stimulation sites. Pre-operative computed tomography images were registered with pre-operative magnetic resonance images by identifying matching anatomical landmarks in computed tomography and magnetic resonance images. The landmarks that were chosen were the anterior commissure, posterior commissure, pontomesencephalic junction, fastigium and trigeminal nerves. These landmarks were used to calculate a rigid-body or thin-plate splines transformation (MINC register, http://www.bic.mni.mcgill.ca/ServicesSoftware). Microelectrode recording coordinates aligned to the pre-operative computed tomography images were transformed to the pre-operative magnetic resonance images. Stimulation sites were determined by identifying hypo-intense lead contacts on post-operative computed tomography images. Post-operative computed tomography images were registered to pre-operative computed tomography images with a mutual information-based rigid transformation using the fMRIB Software Library[48]. For patients in this report, the final stimulation electrodes were placed in the caudal ($n = 7$), mid ($n = 3$) or rostral PPN ($n = 1$). All electrode placements resulted in alleviation of clinical symptoms and will be described in detail elsewhere.

Spike detection and sorting. Spikes were detected and sorted using the Wave Clus package[49] for MATLAB (Mathworks) with additional custom routines. Recordings were filtered using a zero phase distortion 400–3,000-Hz second-order elliptic filter. Spikes were detected as excursions of the filtered signal above an amplitude threshold set to

$$\text{Thr} = 5\sigma_n; \sigma_n = \text{median}\left\{\frac{|x|}{0.6745}\right\}$$

where x is the bandpass-filtered signal and σ_n is an estimate of the s.d. of the background noise.

Spike shapes were extracted (0.5 ms before spike peak to 1 ms after peak), and wavelet coefficients were calculated using a four-level decomposition with Haar wavelets. Spikes from individual neurons were separated using a superparamagnetic clustering algorithm in the Wave Clus package. Clusters were merged if the average spike waveform of the clusters was similar by visual inspection and merging did not increase the proportion of interspike intervals less than 1.25 ms. We excluded units with a mean waveform that that did not have a typical action potential appearance (depolarization and hyperpolarization) and units with 50 Hz (line noise) oscillations.

The signal-to-noise ratio of each unit was calculated as

$$\text{SNR} = \frac{\max\{|s|\}}{\text{median}\left\{\frac{|\hat{x}|}{0.6745}\right\}}$$

where s is the mean spike waveform of the unit, and $\max(|s|)$ is the maximum absolute amplitude of the mean waveform, and $\hat{x}$ are the points in the signal that are not part of the extracted spike waveforms. We studied units with SNR above 4, as these were considered to be well-isolated[50], based on the lower cell density in human subcortical regions compared to rats[51].

Spike duration of each neuron was calculated as the width of the average spike waveform at half-maximal amplitude. We divided neurons into two groups: narrow-spike neurons with spike duration less than 0.225 ms, and wide-spike neurons with spike duration above 0.225 ms (**Supplementary Fig. 1**). To assess differences in discharge characteristics of wide-spiking and narrow-spiking neurons, we compared the mean firing rate and burst statistics for narrow-spiking and wide-spiking neurons pooled across all patients.

For the cross-correlation analysis, we separated pairs of neurons into three categories: (1) narrow-narrow (two narrow-spiking neurons have correlated firing), (2) narrow-wide (one wide-spiking neuron and one-narrow spiking neuron have correlated firing), and (3) wide-wide (two wide-spiking neurons have correlated firing).

Spike train analysis. Spike times were used to calculate mean firing rate and burst statistics for each neuron. We calculated mean firing rate as the number of spikes in the recording duration divided by the duration of the recording. Four methods were used to assess bursting: the burst index, the L-statistic, the Poisson surprise method and the interspike interval (ISI) coefficient of variation. For each of these measures of bursting, a higher value indicates more bursting. To calculate the burst index, an ISI histogram was calculated (bin size = 5 ms), and the burst index was calculated as the mean ISI divided by the modal (most common) ISI. To calculate the L-statistic for a given spike train, the mean ISI of the spike train was calculated, and the spike train was rebinned into segments of this duration. This created a sequence of spike counts per bin, denoted by P_n, where n is the bin number. The L-statistic is the number of distinct values taken by the rebinned process P_n. If a neuron is bursty, its P_n will attain large values (many spikes per mean ISI). The Poisson "surprise" method[52] was used to calculate the proportion of spikes that fired in bursts. In this method, bursts were detected by identifying sequences of consecutive spikes that were highly unlikely to occur by chance, under the assumption of a random (Poisson) spike train. The measure of improbability of observing the burst was calculated as $S = -\log P$, where P is the probability that, in a random (Poisson) spike train having the same average spike rate r as the spike train studied, a given time interval of length T contains n or more spikes. P is given by Poisson's formula, as

$$P = e^{-rT}\sum_{i=n}^{\infty}\frac{(rT)^i}{i!}$$

The ISI coefficient of variation for a given spike train is calculated as $CV = \sigma_{ISI} / \mu_{ISI}$, where σ_{ISI} is the s.d. of the ISIs of the spike train, and μ_{ISI} is the mean ISI.

To evaluate correlated activity of pairs of neurons, we calculated the cross-correlogram of the spike train for each neuron with 1-ms bins, at up to 200-ms lag. This equated to shifting the spike train of one neuron relative to the other spike train by between −200 and 200 ms, at 1-ms intervals, and calculating the correlation between the spike trains at each step. To detect significant peaks in the cross-correlogram, we convolved the cross-correlogram with a partially hollowed window of 11-ms duration, with a hollowed fraction of 0.42 (ref. 53). This produced a predicted cross-correlogram that was used to calculate the probability of obtaining the observed number of counts or greater in each bin of the original cross-correlogram. We tested for significant peaks in the cross-correlogram at short time lags (between –5 and 5 ms). Significant peaks were determined at the $P = 0.01$ level (Bonferroni corrected for the number of bins tested in each cross-correlogram).

Activity during passive movement and imagined gait. To assess changes in neuron firing rate during passive movement and imagined gait, we calculated the firing rate of each neuron in each 1-s interval from the start of the recording to the end of the recording. We then assessed if the firing rates of each neuron were increased, decreased, or unchanged during passive movement or imagined gait compared to the resting condition. We pooled neurons across all patients, and the proportion of narrow-spiking and wide-spiking neurons that increased, decreased, or did not change their firing rate was calculated for passive movement and for imagined gait.

We studied changes in the strength of synchronous discharge of multiple neurons during passive movement and imagined gait by measuring changes in the height of the cross-correlogram peak. The cross-correlograms were first normalized

$$\hat{R}_{ij} = \frac{R_{ij}}{\sqrt{n_i n_j}}$$

where R_{ij} is the original cross-correlogram between units i and j, n_i is the number of spikes that unit i fired, and n_j is the number of spikes that unit j fired. The cross-correlation strength was then given by the value of the normalized cross-correlogram at the peak lag (lag between correlated firing of the two units in milliseconds)

$$\text{correlation strength} = \hat{R}_{ij}(\tau_{\text{peak}})$$

where τ_{peak} is the peak lag. Changes in cross-correlation strength during passive movement or imagined gait in excess of 25% of the resting state correlation strength were considered significant.

Local field potential analysis. To investigate changes in the ratio of alpha power (6–12 Hz) to beta power (12–30 Hz) with recording depth, periods of noise were identified and excluded, and then the power spectral density (PSD) was estimated using Welch's method of averaging over multiple overlapping time windows. We used a window size of 1 s and window step of 0.5 s. Total power in the alpha and beta bands was then summed from the PSD and the alpha/beta ratio calculated for each recording. We also compared the alpha and beta power, and the alpha/beta power ratio, between baseline and imagined gait or movement, using the Welch power spectral density method.

Phase locking of spikes to local field potential. Local field potential (LFP) was extracted from each recording by first down-sampling the recording to 512 Hz then band-pass filtering the signal in the 6–100-Hz band using a linear-phase-response discrete-time finite impulse response filter. A high filter order (1,000) was used to isolate narrow sub-bands of the LFP to distinguish, for example, high alpha oscillations (10–12 Hz) from low beta oscillations (12–20 Hz). The filtered signal was Hilbert transformed to extract the signal phase, and then the spike phase distribution (that is, the LFP phase at the time each spike occurred) for each unit in the recording was tested for non-uniformity using the Rayleigh test for circular data with the significance level set to $P = 0.01$. The LFP and spike times were analyzed over narrow frequency bands (the high frequency cutoff of each band was equal to the low frequency cutoff increased by 11%) and short time windows (2 and 4 s) to facilitate detection of periods of transient phase locking at potentially restricted frequencies. Frequency and time windows were overlapped by 50% to reduce the risk of false negative detections at window edges. For each unit, a phase locking index was calculated; this index represents the proportion of time that the unit was phase locked in a given time period and given frequency range. For example, if 20 out of 1,000 time-frequency window Rayleigh tests were significant, then the phase locking index for that time period and frequency range would equal 0.02. Results were visualized on color-coded maps of frequency versus time where brighter colors indicated stronger phase locking. Phase locking indices were also calculated separately for each unit for periods of rest and during motor tasks in the alpha (6–12 Hz) band. These phase locking indices were used to calculate summary statistics and to test for differences in phase locking between PPN regions and motor tasks.

Statistics. No statistical test was used to determine sample size a priori and our sample sizes are similar to those used in previous publications. Firing rates during passive movement and imagined gait were compared to baseline for each neuron using the Wilcoxon rank-sum test (significance level = 0.05). Significance of LFP power and phase locking changes between rest and motor tasks were assessed using the Wilcoxon signed rank test. All statistical tests were two-sided. Given the task design and the methods used for analysis of the data, no blinding and randomization were required.

47. Coyne, T. *et al.* Rapid subthalamic nucleus deep brain stimulation lead placement utilising CT/MRI fusion, microelectrode recording and test stimulation. *Acta Neurochir. (Wien)* **99** (suppl.): 49–50 (2006).
48. Smith, S.M. *et al.* Advances in functional and structural MR image analysis and implementation as FSL. *Neuroimage* **23** (suppl. 1): S208–S219 (2004).
49. Quiroga, R.Q., Nadasdy, Z. & Ben-Shaul, Y. Unsupervised spike detection and sorting with wavelets and superparamagnetic clustering. *Neural Comput.* **16**, 1661–1687 (2004).
50. Stratton, P. *et al.* Action potential waveform variability limits multi-unit separation in freely behaving rats. *PLoS ONE* **7**, e38482 (2012).
51. Hardman, C.D. *et al.* Comparison of the basal ganglia in rats, marmosets, macaques, baboons, and humans: volume and neuronal number for the output, internal relay, and striatal modulating nuclei. *J. Comp. Neurol.* **445**, 238–255 (2002).
52. Legéndy, C.R. & Salcman, M. Bursts and recurrences of bursts in the spike trains of spontaneously active striate cortex neurons. *J. Neurophysiol.* **53**, 926–939 (1985).
53. Stark, E. & Abeles, M. Unbiased estimation of precise temporal correlations between spike trains. *J. Neurosci. Methods* **179**, 90–100 (2009).

doi:10.1038/nn.3642